Direct and semi-direct capture in low-energy (n, γ) reactions of neutron-rich tin isotopes and its implications for r-process nucleosynthesis

S. Chiba,[1] H. Koura,[1] T. Hayakawa,[2,3] T. Maruyama,[1] T. Kawano,[4] and T. Kajino[3]

[1]*Advanced Science Research Center, Japan Atomic Energy Agency, Tokai, Naka, Ibaraki 319-1195, Japan*
[2]*Kansai Photon Science Institute, Japan Atomic Energy Agency, Kizu, Kyoto 619-0215, Japan*
[3]*National Astronomical Observatory, Osawa, Mitaka, Tokyo 181-8588, Japan and Department of Astronomy, School of Science,*
University of Tokyo, Hongo, Bunkyo-ku, Tokyo 113-0033, Japan
[4]*Theoretical Division, Los Alamos National Laboratory, Los Alamos, New Mexico 87545, USA*

The direct and semi-direct (DSD) components of the neutron capture cross sections are calculated for a series of tin isotopes by employing a single-particle potential (SPP) that gives a good reproduction of the known single-particle energies (SPEs) over a wide mass region. The results are compared with the Hauser-Feshbach (HF) contribution in the energy region of astrophysical interest. The calculated result shows that the HF component drops off rapidly for isotope ^{132}Sn and toward more neutron-rich ones, whereas the DSD component decreases only smoothly and eventually becomes dominant. This result is consistent with those of previous studies, but the dependence of the DSD cross section on the target mass number is a feature of the present SPP that gives a smooth variation of SPEs. As a consequence, the direct portion of the DSD component gives the largest contribution to the total (n, γ) cross section for neutron-rich isotopes below a few MeV. Therefore, the direct capture process modifies the astrophysical (n, γ) reaction rates to a great extent. The semi-direct component, however, gives a negligible contribution to the astrophysical reaction rates, but its impact is significant above several MeV. The reason for the difference in isotopic dependence between the HF and DSD components is discussed, and its implication for r-process nucleosynthesis is given.

I. INTRODUCTION

The neutron capture reaction rate on neutron-rich unstable isotopes far from the β-stability line is essential for rapid neutron capture nucleosynthesis (r-process), which is considered to occur in supernova explosions (e.g., see Refs. [1–7]). The nuclear reaction flows in the r-process occur in the vicinity of the neutron drip line. Mathews *et al.* [8] pointed out that there might be circumstances where the direct capture process is important in the neutron capture reactions relevant to the r-process.

It is known that there are three major mechanisms in neutron capture by nuclei, namely, compound (including resonances) and direct and semi-direct (DSD) processes. Normally, the direct process is not considered to be very important because its cross section is much smaller than the compound capture cross sections, which give the dominant contribution at energies below several MeV, and is also smaller than that of the semi-direct process at energies above. For this reason, many of the comprehensive programs used to calculate nuclear cross sections (or nuclear data) adopt a simple estimate of the direct and semi-direct cross sections in terms of pre-equilibrium γ emission [9] as well as Hauser-Feshbach (HF) theory (e.g., Refs. [10,11]). Such an approach can be justified when it is applied to the nuclei in the vicinity of the stability line. However, in the neutron-rich region relevant to the r-process, the neutron separation energy tends to be smaller, so the compound nuclei may not have enough excitation energy, which reduces the level density, to compete with the compound elastic process. Then, the compound capture cross section may be significantly suppressed, and the significance of the direct capture becomes relatively high even at low energies

where the pre-equilibrium picture is obviously incorrect. We here point out an example of a direct neutron capture reaction measurement of Si isotopes, which contributes to the cosmochronology of presolar SiC grains in primitive meteorites [12].

The neutron magic numbers affect the final mass distribution of products in the r-process, where the capture cross sections have minima. Astronomical observations of metal-deficient stars reported a "universal" abundance distribution of the r nuclei in the same mass region [13] but indicated that relative abundances between different mass regions caused by the neutron magic number $N = 82$ on the neutron drip line are different [14]. Therefore, an unstable nucleus ^{132}Sn ($N = 82$) is key for understanding the r-process. Rauscher *et al.* [15] presented clearly the role of the direct neutron capture reaction on tin and lead isotopes by calculations. They have employed three different models for the single-particle potentials (SPPs), namely, the Hartree-Fock-Bogoliubov model, relativistic mean field theory, and the macroscopic-microscopic finite-range droplet model. Predictions based on different models sometimes disagree up to several orders of magnitude, showing a clear need of a search for SPPs that can reproduce the single-particle energies (SPEs) correctly. Goriery [16] has carried out a comprehensive calculation of the neutron direct capture cross sections using a level density description and average spectroscopic factors. This approach may certainly be a way to tackle this problem in a systematic way. However, it is evident that the precise nuclear structure effect present in the direct capture of magic-number nuclei is somewhat washed out in it. These results suggest that more work needs to be done in this direction.

The recent progress in radioactive beam techniques has enabled us to measure (d, p) reaction cross sections on important r-process unstable nuclei [17]. Therefore, we carry out a systematic calculation of both direct and semi-direct (DSD) cross sections in the present work to improve the prediction of the neutron capture reaction rate on the tin isotopes. The contribution of the semi-direct reaction was ignored in most of the previous work [8,15,16,18], since it has been known that the cross section of the semi-direct reaction is small relative to that of the direct reaction below several MeV. The semi-direct cross section was included here to calculate the capture cross section up to 20 MeV to cover a range wide enough for many other applications consistently. In the present study, we adopt a single-particle potential that gives a good reproduction of the known single-particle energies over a wide mass region. We also perform HF model calculations [19–21] and consider whether the inversion of the HF and direct cross sections occurs at the neutron-rich isotopes. The implication of the importance of direct capture for r-process nucleosynthesis is also investigated.

This paper is organized as follows. The computational method is presented in Sec. II. Section III is devoted to comparisons of the present results with experimental data (both SPE and capture cross sections) and results calculated by HF theory. The astrophysical reaction rates are calculated for ^{132}Sn by using both the HF and HF + DSD data, and results of a dynamical r-process calculation with them are compared. The implication for r-process nucleosynthesis is also discussed. The summary of this work is given in Sec. IV.

II. CALCULATION OF THE CROSS SECTIONS

For spherical even-even nuclei considered in this work, the $E1$ part of the DSD cross section can be written as a sum of various transitions from the initial (scattering) states to the final (bound) states [22–24]:

$$\sigma = \frac{8}{9}\pi\frac{\mu}{\hbar^2 k^3}\sum_{\ell j n'\ell' j'} U_{n'\ell'j'}^2 k_\gamma^3 Z\left(\ell j \ell' j'; \frac{1}{2}1\right)^2$$
$$\times |T_d(\ell, j \to n', \ell', j') + T_{sd}(\ell, j \to n', \ell', j')|^2, \quad (1)$$

where μ denotes the reduced mass, k the wave number of the projectile, k_γ the wave number of emitted γ rays, and $U_{n'\ell'j'}^2$ the BCS vacancy probability of the capture state. Here, the symbols ℓ, j designate the orbital angular momentum and $\ell \pm 1/2$ of initial scattering states and n', ℓ', j' are the principal quantum number, orbital angular momentum, and $\ell' \pm 1/2$ of the states of the final nucleus to which neutrons are captured, respectively. The symbol Z determines the coupling of angular momenta. We assumed here that all the γ transitions are isospin allowed, so the minor contributions from the $M1$ transition and higher multipolarities are ignored.

The direct and semi-direct amplitudes T_d and T_{sd} are given for neutron-induced reactions as

$$T_d(\ell, j \to n', \ell', j') = \bar{e}\mathcal{I}_d(n'\ell'j'; \ell j), \quad (2)$$

$$T_{sd}(\ell, j \to n', \ell', j') = -\frac{3}{\langle r^2\rangle}e\mathcal{I}_{sd}(n'\ell'j'; \ell j)\mathcal{Z}_{sd}. \quad (3)$$

Here, $\bar{e}$ denotes the effective charge, which is given as $\bar{e} = -Ze/A$ for neutron-induced reactions, and $\langle r^2\rangle$ is the mean-square potential radius. The overlap integrals are obtained as

$$\mathcal{I}_d(n'\ell'j'; \ell j) = \langle u_{n'\ell'j'}|r|\varphi_{\ell j}\rangle, \quad (4)$$

$$\mathcal{I}_{sd}(n'\ell'j'; \ell j) = \langle u_{n'\ell'j'}|h(r)|\varphi_{\ell j}\rangle, \quad (5)$$

where $u_{n'\ell'j'}$ and $\varphi_{\ell j}$ denote the wave functions of the bound and scattering states, respectively.

The particle-vibration coupling function, $h(r)$, is given as

$$h(r) = V_1 r f(r) - i W_1 4ar\frac{d}{dr}f(r) \quad (6)$$

for the complex coupling proposed by Potkar [25] (see also Ref. [23]) (which we employed with $V_1 = 75$ MeV and $W_1 = 140$ MeV fixed) and as

$$h(r) = -\frac{\langle r^2\rangle}{3}V_1\frac{d}{dr}f(r) \quad (7)$$

for surface coupling employed traditionally.

The quantity $\mathcal{Z}_{sd}$ contains the transition matrix element between the dipole and ground states, which can be related to experimentally observed quantities through the giant dipole resonance (GDR) sum rule:

$$\mathcal{Z}_{sd} = \frac{\frac{(NZ)^2}{2A^3}|\langle\Psi_{10}(\xi')|\rho_0'|\Psi_{00}(\xi')\rangle|^2}{E_\gamma - E_r + i\frac{1}{2}\Gamma_r} = \frac{\frac{1}{16\pi}\left(\frac{e^2}{\hbar c}\right)^{-1}\frac{\sigma_r^{\max}\Gamma_r}{AE_r}}{E_\gamma - E_r + i\frac{1}{2}\Gamma_r}, \quad (8)$$

where E_γ is the energy of emitted γ rays, which can be given as a difference of the incident particle energy E and the binding energy $\epsilon_{n'\ell'j'}$ of the captured state: $E_\gamma = E - \epsilon_{n'\ell'j'}$. Finally, the symbols E_r, Γ_r, and $\sigma_r^{\max}$ are the GDR parameters (the position, width, and peak height of the GDR).

The structure of these formulas gives us some details of the low-energy behavior of the DSD cross sections. They can be summarized as follows: 1. Eq. (1) is proportional to the third power of $k_\gamma = \frac{E - \epsilon_{n'\ell'j'}}{\hbar c}$, which is $\sim \frac{|\epsilon_{n'\ell'j'}|}{\hbar c}$ at low energy. It is noted that the direct capture cross section actually varies linearly with the binding energy of the final bound state [26]. Therefore, the DSD cross section depends strongly on the binding energy at low energies, which is sensitive to the precise structure of the single-particle levels and therefore to the single-particle potential. 2. The coefficient $Z(\ell j \ell' j'; \frac{1}{2}1)$ gives the selection rule of the angular momenta. For the orbital angular momenta, it gives a restriction that $\ell' = \ell \pm 1$. Therefore the bound s state ($\ell' = 0$) can couple to only the initial (unbound) p wave ($\ell = 1$), the bound p state to the initial s and d waves, etc.

To calculate the overlap integrals [Eqs. (4) and (5)], we need to specify an optical model potential (OMP) and a SPP. In this work, we adopted the Koning-Delaroche's OMP [27] and Koura-Yamada's SPP [28] (KY-SPP) for the scattering and bound states, respectively, for the following reasons. The Koning-Delaroche OMP was parametrized by considering a huge number of scattering observables including low-energy ones, so it is considered to be one of the best spherical nucleon OMP at present. Similarly, KY-SPP was determined by considering the single-particle levels in the vicinity of 15 doubly magic or magic-submagic nuclei ranging from ^{4}He
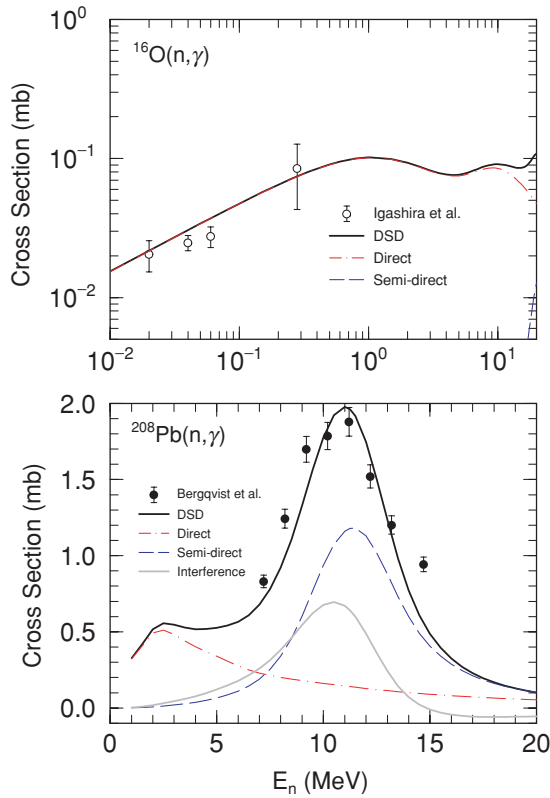
FIG. 1. (Color online) The (n, γ) cross sections of ^{16}O (top panel) and ^{208}Pb. The present DSD and direct and semi-direct cross sections are compared with experimental data [30,31]. In the lower panel, the interference term between the direct and semi-direct mechanisms is also shown.

to ^{208}Pb. This potential is an extension of the Woods-Saxon potential including two new parameters modifying the surface structure of the potential. The use of different potentials has the advantage that physical quantities, and therefore the wave functions, are consistent with observed data in both the negative and positive channels. The GDR parameters required in the calculations of the semi-direct cross sections are determined according to D'Arigo's systematics [29].

As a validation of the present method, we compare the neutron capture cross sections of ^{16}O and ^{208}Pb in Fig. 1. The present approach reproduces the measured data [30,31] fairly well without parameter adjustment. It is clearly seen that the direct process is dominant for ^{16}O over the entire energy range, whereas the relative strength of the direct and semi-direct processes are interchanged at around 7 MeV for ^{208}Pb.

III. RESULTS AND DISCUSSION

Figure 2 shows neutron single-particle levels in the vicinity of ^{132}Sn. The single-particle energies above the $N = 82$ gap are obtained as the neutron separation energy necessary to bring the nucleus from the corresponding single-particle states of ^{133}Sn to the ground state ^{132}Sn, whereas those below the $N = 82$ gap are given as the neutron separation energy from
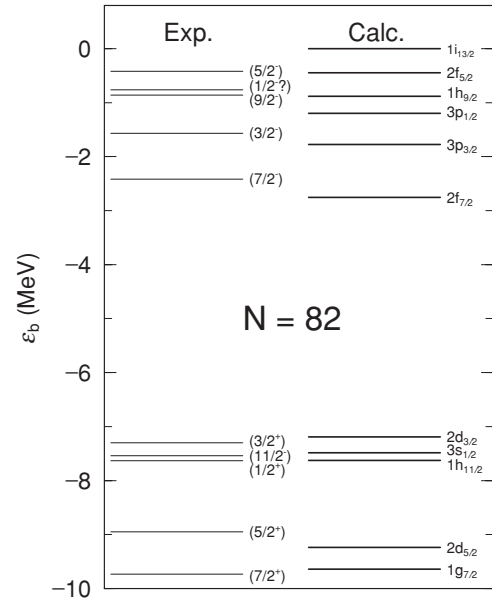

FIG. 2. Neutron single-particle energies in the vicinity of ^{132}Sn. The binding energies calculated with Koura-Yamada's SPP (right) are compared to the corresponding experimental values [32,33] (left). See text for details.

the ground state of ^{132}Sn to the corresponding single-hole states of ^{131}Sn [28]. Calculated binding energies with Koura-Yamada's SPP (right) are compared to the corresponding experimental values [32,33] (left). The levels calculated predict a somewhat narrower gap at $N = 82$, but the single-particle energies of the unfilled levels are reproduced with an accuracy of about 300 keV on average. As the low-energy DSD cross section is proportional to $|\epsilon_{n'\ell'j'}|$, it is important to reproduce the single-particle energies to this accuracy. The J^π assignment of the experimental levels [32,33] is still ambiguous, but they clearly exhibit a large $N = 82$ gap of around 5 MeV between the $3/2^+$ and $7/2^-$ levels.

It is also very important, as we will see later, to predict the presence of $3p_{3/2}$ and $3p_{1/2}$ states, which can couple to the s wave of the scattering wave function. Owing to the large energy gap, particle excitation requires an energy of several MeV (gap + pairing energies). Therefore, it can be said that the frequently employed pre-equilibrium γ-emission model cannot be used for incident energies below several MeV for this nucleus. We present calculated and measured excited levels in Fig. 3. We would like to stress that our result successfully reproduces the measured levels [32,33].

Figure 4 shows the calculated HF and DSD cross sections for ^{122}Sn (left panel) and ^{132}Sn (right panel) in the energy region of 1 keV to 20 MeV. The HF cross sections were calculated with the GNASH code [11]. For ^{122}Sn, the HF cross section is dominant below several MeV; it is larger than the DSD one by about two orders of magnitude. In the DSD component, the direct cross section is dominant below several MeV, and it has smooth decreasing characteristics. The semi-direct component has a peak above 10 MeV. However, the entire cross section is dominated by the low-energy HF component.
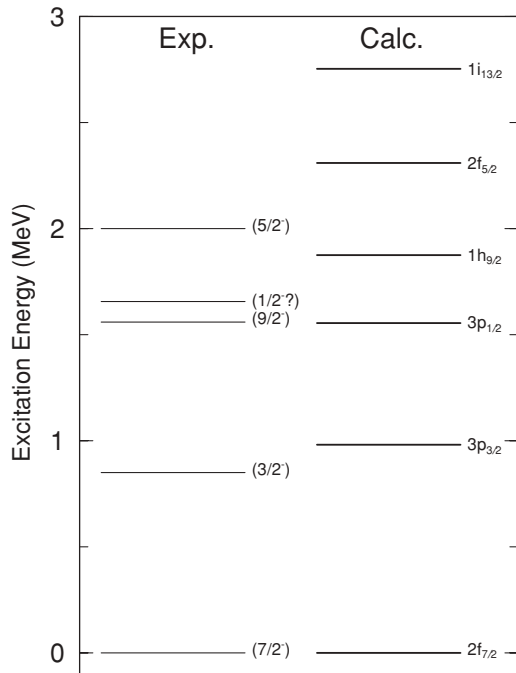
FIG. 3. Excited states in ^{133}Sn corresponding to the single-particle neutron states. The experimentally known levels [33] are shown in the left column; the predicted ones with KY-SPP are shown in the right column.

FIG. 5. (Color online) The DSD (n, γ) cross sections of ^{132}Sn to various final states of the composite nucleus.

whereas it is 2.47 MeV for ^{132}Sn. If we subtract the pairing energy (about 1.2 MeV) of the compound nucleus from them, there is not much excitation energy left for ^{133}Sn. This reduces the level density of the compound nucleus drastically that leads to reduced HF cross section.

Next, the state-wise DSD cross sections of ^{132}Sn are plotted in Fig. 5. Here, cross sections leading to all the possible final states in ^{133}Sn are shown. There is a remarkable feature in this figure. The cross sections to the $2f_{7/2}$, $1h_{9/2}$, $2f_{5/2}$, and $1i_{13/2}$ states are smaller than 1 nb at 1 keV, and they increase monotonically as the incident energy increases. In contrast, the cross sections leading to the $3p_{3/2}$ and $3p_{1/2}$ states have an order of 0.1 to 1 mb at 1 keV, and they decrease slightly but keep the level of 0.1 mb up to several MeV. Therefore, it is understood that the DSD cross section of ^{132}Sn at low energy has a dominant contribution from the p states in the final nucleus below several hundred keV. The reason is obvious. Because of the spin-selection rule, the final p states are the only states that can couple to the initial s-wave scattering state that is dominant at a low-energy region. All the other states can couple only to higher partial waves, so the overlap

In contrast, the HF cross section for ^{132}Sn is much smaller than that of ^{122}Sn, and it is also smaller than the DSD cross section below 1 MeV. In this energy region, the DSD cross section is due mostly to the direct one, so the low-energy (n, γ) reaction of ^{132}Sn is dominated by the direct process. It is important to note that, although the HF cross sections of ^{122}Sn and ^{132}Sn differ by about two orders of magnitude, the direct cross sections of these nuclei differ only by a factor of 2. The difference of the HF cross sections between ^{122}Sn and ^{132}Sn is caused by the difference of the neutron separation energy of the compound nuclei. For ^{122}Sn, it is 5.95 MeV,
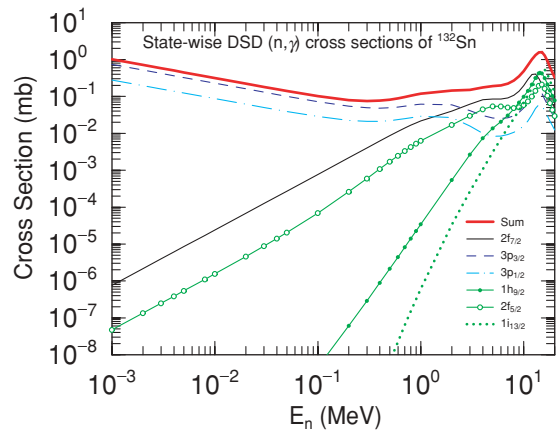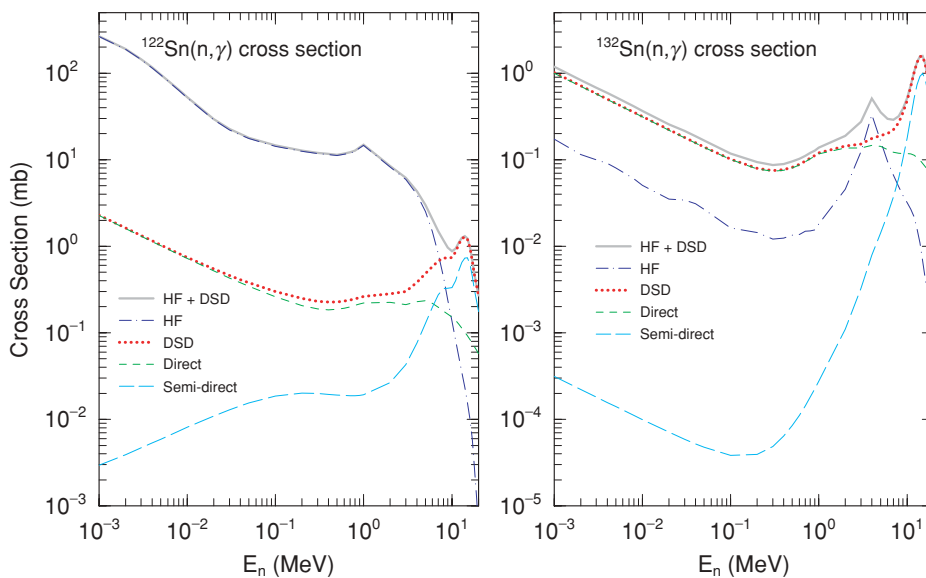

FIG. 4. (Color online) Neutron capture cross section of ^{122}Sn (left panel) and ^{132}Sn (right panel) in the energy range from 1 keV to 20 MeV. The HF + DSD (solid line), HF (dash-dotted), DSD (dots), direct (dashed), and semi-direct (long-dashed) components are shown. Note the difference of two orders of magnitude in the scale of the vertical axes.
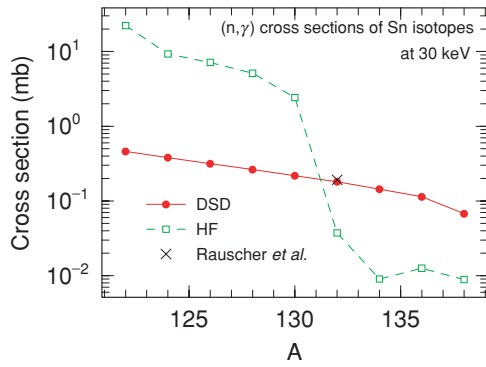
FIG. 6. (Color online) The calculated neutron capture cross sections at incident neutron energy of 30 keV. The HF cross section is shown by the open squares connected with a dashed line and the DSD one by filled circles with a solid line. The cross denotes the best estimate for the direct (n, γ) cross section of ^{132}Sn by Rauscher *et al.* obtained using the experimental single-particle energies [15].

integral is much smaller than that between bound p states and an unbound s wave. Therefore, it is essential for the SPP to predict the presence and positions of the p states. As long as we have these contributions, the low-energy DSD cross section (which is nearly equal to the direct one) can be kept to the order of 0.1 to 1 mb, which can be much larger than the HF cross section for nuclei such as ^{132}Sn. There must be more levels for ^{122}Sn available as the final states, so the difference of a factor of 2 in the direct cross sections of ^{122}Sn and ^{132}Sn is understandable. However, we expect that they do not differ by much as long as the direct process to the p states is present.

In Fig. 6, we plot neutron capture cross sections of even-even tin isotopes at $E_n = 30$ keV. The HF cross section decreases as the mass number increases and shows a drastic decrease when going from ^{130}Sn to ^{132}Sn. This trend is completely correlated with the values of neutron separation energies. In contrast, the DSD cross section decreases only modestly, and it exceeds the HF cross section at ^{132}Sn. Therefore, we see that the inversion of the HF and DSD cross sections indeed occurs at the border of the $N = 82$ magic number for the neutron-rich tin isotopes (and probably its vicinity). The gradual decrease of the direct cross sections in our calculation is different from the more-rapid mass-number dependence of Rauscher *et al.* [15], probably because of the stability of the single-particle energies calculated by KY-SPP. The cross symbol denotes a result calculated by Rauscher *et al.* using experimental level energies as their best estimate of the direct (n, γ) cross section of ^{132}Sn [15]. Our result, without such an adjustment, is in fair agreement with their value.

The astrophysical reaction rates (ARRs) of ^{132}Sn, defined as $R = N_A \langle \sigma v \rangle$, where N_A stands for the Avogadro constant, are calculated based on the HF and HF + DSD cross sections and are displayed in Fig. 7 as a function of temperature T_9 (in 10^9 K). As shown, the HF rate is smaller than the HF + DSD rate by about a factor of 8 in the whole temperature region relevant to the r-process. We have made a full nuclear reaction network calculation including neutrino-induced reactions [6] with a hydrodynamical trajectory by employing both reaction rates. We have adopted a single trajectory from a fully general
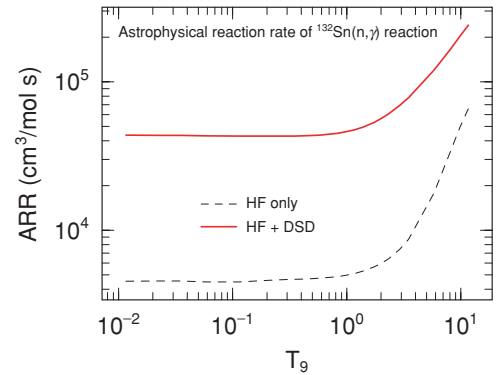
relativistic simulation of the neutrino-driven wind [5], which has a relatively short expansion time of 5.1 ms owing to the intense neutrino flux assumed. The reaction network is ignited in expanding matter when the temperature T_9 drops to 9. From this point, the temperature drops rapidly, then becomes nearly constant at $T_9 \sim 0.62$. We start from a soup consisting of neutrons, protons, and electrons with an electron fraction $Y_e (= Y_p)$ of 0.42. This value was taken from Ref. [5]. The ratio of ^{132}Sn abundances obtained with both ARRs is shown in Fig. 8. There is a clear deviation from unity in the abundance of ^{132}Sn. The abundance with the HF rate is larger than the one with the HF + DSD rate by about a factor of 3.6 up to around 0.6 s and a smaller but nonzero difference persists beyond. This means that the matter flow at the early stage of the r-process is sensitive to the adopted reaction rate, which may alter the initial pattern of the seed nuclei. Although the final abundance does not seem to depend on the adopted reaction rates very much, it can be said that it is important to employ accurate reaction rates as much as possible to
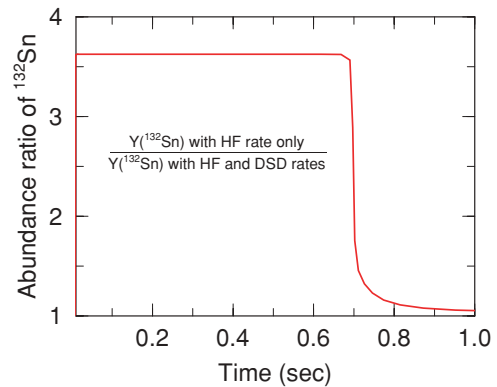

FIG. 7. (Color online) The astrophysical reaction rates for the ^{132}Sn(n, γ) reaction as a function of temperature T_9 (in 10^9 K). The ARR calculated with the HF contribution only is shown by the dashed line; one with HF + DSD contributions are shown by the solid line.

FIG. 8. (Color online) Abundance ratio of the ^{132}Sn nucleus during an an r-process event. The ratio is given as the abundance of ^{132}Sn where the HF reaction rate for the ^{132}Sn(n, γ) reaction is used over that where HF and DSD rates are used. Other reaction rates and astrophysical conditions were kept equal for both calculations. The horizontal axis is the time after the temperature has dropped to $T_9 = 9$.

understand the detailed mechanism of the matter flow during *r*-process nucleosynthesis. This confirms the importance of direct neutron capture for neutron-rich tin isotopes.

IV. CONCLUDING REMARKS

We calculate direct and semi-direct neutron capture cross sections for a series of even-even tin isotopes. We adopt the Koura-Yamada's single-particle potential, which gives a good reproduction of the known single-particle energies over a wide mass region. Our calculation agrees well with that of Rauscher *et al.* [15] using the experimental single-particle energies, which were regarded as reference data in their work. In case of tin, it is essentially important to be able to predict the energies of *p* states that can couple to an initial *s* wave. We also demonstrated that this approach including the KY-SPP reproduced the measured reaction on ^{16}O and ^{208}Pb without parameter adjustment. We believe that this fact, together with a comparison of the DSD cross sections in other stable nuclei, generally verifies the use of KY-SPP for calculation of neutron DSD cross sections over wide regions of mass number and N/Z ratio.

The calculated result shows that the HF component, which is known to be dominant for isotopes in the vicinity of the stability line, drops off rapidly for the isotope ^{132}Sn and toward more neutron-rich ones, whereas the DSD component decreases only smoothly. The latter is a feature of the DSD cross sections predicted with KY-SPP. Inclusion of the DSD (or mostly direct) neutron capture alters the astrophysical (n, γ) reaction rate by as much as a factor of 8 for nuclei such as ^{132}Sn. These results are consistent with those of previous studies. It was shown that the matter flow during the early stage of the *r*-process is sensitive to the adopted neutron capture rates. The semi-direct capture process is dominant above several MeV, and interference between the direct and semi-direct processes is important for medium to heavy nuclei. Although it was shown that the contribution of the semi-direct capture process is small in astrophysical energies, we included it quantitatively here for the purpose of extending it to other application purposes in a unified way.

[1] B. S. Meyer, G. J. Mathews, W. M. Howard, S. E. Woosley, and R. D. Hoffman, Astrophys. J. **399**, 656 (1992).

[2] S. E. Woosley, J. R. Wilson, G. J. Mathews, R. D. Hoffman, and B. S. Meyer, Astrophys. J. **433**, 229 (1994).

[3] Y.-Z. Qian, P. Vogel, and G. J. Wasserburg, Astrophys. J. **494**, 285 (1998).

[4] J. J. Cowan, B. Pfeiffer, K.-L. Kratz, F.-K. Thielemann, C. Sneden, S. Burles, D. Tytler, and T. C. Beers, Astrophys. J. **521**, 194 (1999).

[5] K. Sumiyoshi, H. Suzuki, K. Otsuki, M. Terasawa, and T. Yamada, Publ. Astron. Soc. Jpn. **52**, 601 (2000).

[6] M. Terasawa, K. Sumiyoshi, T. Kajino, G. Mathews, and I. Tanihata, Astrophys. J. **562**, 470 (2001).

[7] J. W. Truran, J. J. Cowan, C. A. Pilachowski, and C. Sneden, Publ. Astron. Soc. Pac. **114**, 1293 (2002).

[8] G. J. Matthews, A. Mengoni, F.-K. Thielemann, and W. A. Fowler, Astrophys. J. **270**, 740 (1983).

[9] J. M. Akkermans and H. Gruppelaar, Phys. Lett. **B157**, 95 (1985).

[10] A. J. Koning, S. Hilaire, and M. Duijvestijn, NRG Report 21297/04.62741/P FAI/AK/AK, NRG, Petten, the Netherlands, 2004.

[11] P. G. Young, E. D. Arthur, and M. B. Chadwick, LA-12343-MS, Los Alamos National Laboratory, 1992.

[12] K. H. Guber, P. E. Koehler, H. Derrien, T. E. Valentine, L. C. Leal, R. O. Sayer, and T. Rauscher, Phys. Rev. C **67**, 062802(R) (2003).

[13] C. Sneden, J. J. Cowan, D. L. Burris, and J. W. Truran, Astrophys. J. **496**, 235 (1998).

[14] C. Sneden, J. J. Cowan, I. I. Ivans, G. M. Fuller, S. Burles, T. C. Beers, and J. E. Lawler, Astrophys. J. **533**, L139 (2000).

[15] T. Rauscher, R. Bieber, H. Oberhummer, K.-L. Kratz, J. Dobaczewski, P. Möller, and M. M. Sharma, Phys. Rev. C **57**, 2031 (1998).

[16] S. Goriely, Astron. Astrophys. **325**, 414 (1997).

[17] J. S. Thomas, D. W. Bardayan, J. C. Blackmon, J. A. Cizewski, U. Greife, C. J. Gross, M. S. Johnson, K. L. Jones, R. L. Kozub, J. F. Liang, R. J. Livesay, Z. Ma, B. H. Moazen, C. D. Nesaraja, D. Shapira, and M. S. Smith, Phys. Rev. C **71**, 021302(R) (2005).

[18] A. Mengoni, T. Otsuka, and M. Ishihara, Phys. Rev. C **52**, R2334 (1995).

[19] T. Nakagawa, S. Chiba, T. Hayakawa, and T. Kajino, At. Data Nucl. Data Tables **91**, 77 (2005).

[20] T. Hayakawa T. Shizuma, T. Kajino, S. Chiba, N. Shinohara, T. Nakagawa, and T. Arima, Astrophys. J. **628**, 533 (2005).

[21] T. Hayakawa, S. Miyamoto, Y. Hayashi, K. Kawase, K. Horikawa, S. Chiba, K. Nakanishi, H. Hashimoto, T. Ohta, M. Kando, T. Mochizuki, T. Kajino, and M. Fujiwara, Phys. Rev. C **74**, 065802 (2006).

[22] J. P. Boisson and S. Jang, Nucl. Phys. **A189**, 334 (1972).

[23] T. Watanabe, L. Bonneau, and T. Kawano, Proc. of the 11th Int. Conf. on Nuclear Reaction Mechanisms, 12–16 June, 2006, Villa Monastero, Varenna, Italy, edited by E. Gadioli, Ricerca Scientifica ed Educazione Permanente Supplemento No. 126, 85 (2006).

[24] L. Bonneau, T. Kawano, T. Watanabe, and S. Chiba, Phys. Rev. C **75**, 054618 (2007).

[25] M. Potkar, Phys. Lett. **B46**, 346 (1973).

[26] A. M. Lane and J. E. Lynn, Nucl. Phys. **17**, 586 (1960).

[27] A. J. Koning and J.-P. Delaroche, Nucl. Phys. **A713**, 231 (2003).

[28] H. Koura and M. Yamada, Nucl. Phys. **A671**, 96 (2000).

[29] T. Belgya, O. Bersillon, R. Capote, T. Fukahori, G. Zhigang, S. Goriely, M. Herman, A. V. Ignatyuk, S. Kailas, A. Koning, P. Oblozhinsky, V. Plujko, and P. Young, IAEA-TECDOC-

1506 (IAEA, Vienna, 2006). Available online at http://www-nds.iaea.org/RIPL-2/.

[30] M. Igashira, Y. Nagai, K. Masuda, T. Ohsaki, and H. Kitazawa, Astrophys. J. **441**, L89 (1995).

[31] I. Bergqvist, D. M. Drake, and D. K. Mc Daniels, Nucl. Phys. **A191**, 641 (1972).

[32] B. Fogelberg and J. Blomqvist, Phys. Lett. **B137**, 20 (1984).

[33] P. Hoff, P. Baumann, A. Huck, A. Knipper, G. Walter, G. Marguier, B. Fogelberg, A. Lindroth, H. Mach, M. Sanchez-Vega, R. B. E. Taylor, P. Van Duppen, A. Jokinen, M. Lindroos, M. Ramdhane, W. Kurcewicz, B. Jonson, G. Nyman, Y. Jading, K.-L. Kratz, A. Wöhr, G. Lovhoiden, T. R. Thorsteinsen, and J. Blomqvist (ISOLDE Collaboration), Phys. Rev. Lett. **77**, 1020 (1996).